Available online at www.sciencedirect.com

ScienceDirect

journal homepage: www.elsevier.com/locate/he

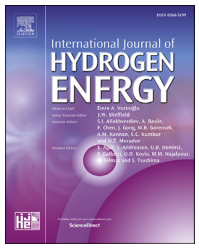

$LaNi_5$ hydride powder flowability as a function of activation and hydrogen content

Maximiliano Melnichuk [a,b,*], *Diego J. Cuscueta* [a,c], *Nicolas Silin* [a,c]

[a] *CONICET: Concejo Nacional de Investigaciones Científicas y Técnicas, Argentina*
[b] *C.N.E.A.: Comisión Nacional de Energia Atomica, Argentina*
[c] *Instituto Balseiro, Centro Atómico Bariloche (C.N.E.A.), Universidad Nacional de Cuyo, Av. E. Bustillo 9500, CP 8400, S.C. de Bariloche, Río Negro, Argentina*

ARTICLE INFO

Article history:
Received 17 January 2017
Received in revised form
21 February 2017
Accepted 22 February 2017
Available online 2 June 2017

Keywords:
Hydride rheology
Powder flowability
Rotating drum
Dynamic angle of repose
Container stress

ABSTRACT

Volume expansion of hydrogen absorbing materials, together with inter-particle friction can cause tension accumulation in hydride containers during absorption. When hydride particles absorb hydrogen there is an important volume increase, in the order of 25%. Particles have to accommodate to the container geometry but this movement is opposed by inter-particle friction. Under certain conditions tensions can build up, compromising the mechanical integrity of the container. This phenomenon needs to be addressed at the design stage to avoid mechanical failure of the container.

Flow behavior of powder materials is a relevant technological field, usually addressed by means of qualitative or quantitative flowability measuring devices. The rotating drum technique, while mainly qualitative, is well established and can be modified into a completely sealed unit. To determine the flowability of a hydride under different activation stages and hydrogen content levels we developed a rotating drum device that can be pressurized with hydrogen or depressurized. We report particle size evolution and flowability measurements of a hydrogen absorbing material ($LaNi_5$) at different stages of activation for both absorbed and desorbed states. The results of the present study show that the flowability of $LaNi_5$ in more dependent on the degree of activation of the sample than on hydrogen absorption state.

Introduction

Hydrogen storage by means of hydrides is an alternative to compressed or liquefied hydrogen storage methods. It has been under study for more than three decades because of some promising characteristics: no need of cryogenic temperatures or high pressures, high energy density and relative safety [1–3].

Generally speaking, hydride materials are synthetized by mechanical alloying or melted under inert gas atmosphere. To achieve a satisfactory reaction performance it is necessary to have a high specific free surface area. This is achieved by reducing the particle size to a range between 1 μm and 15 μm. Size reduction is readily achieved by mechanical alloying, which also causes particle breakage. On the other hand, for the melting process particle, size reduction is achieved through an activation procedure. Given that hydrogen absorbing alloys are fragile, and that there is an important density change of the material during absorption (≈25% swelling) [4,5], the activation process consists of cycling

* *Corresponding author*. Centro Atomico Bariloche, Av. Ezequiel Bustillo 9500, 8400 Bariloche, Argentina. Fax: +54 294 4445299.
E-mail address: mmelnichuk@cab.cnea.gov.ar (M. Melnichuk).
http://dx.doi.org/10.1016/j.ijhydene.2017.02.164
0360-3199/

several times the melted material between hydrogen pressure and vacuum. This results in an effective size reduction of the alloy particles. For lanthanum-nickel based alloys, after 12–15 cycles the particle size distribution is expected to decrease to a point where the material can be considered stabilized to practical uses [6].

Volume expansion of hydride particles causes a tension accumulation in the hydride container that needs to be addressed to avoid mechanical failure. Many studies have been done on this topic, mostly on hydride container prototypes [7–12]. Among horizontal cylindrical containers, McKillip et al. [13] measured the accumulated tension as a function of hydrogen charge at different filling percentages. The maximum stress value reported was 75 MPa for the 100% filling at full hydrogen charge condition. Other authors reported mechanical failure of stainless steel containers due to hydride expansion, measuring stress values above 350 MPa [14,15]. In this sense, Haas and Schütt have shown that the accumulation of mechanical pressure can also be detrimental for the hydrogen uptake capacity of the hydride forming alloy [16]. In a recent study, Heubner et al. [17] introduce the concept of pressure-stress-isotherms in analogy to traditional thermodynamic characterization, by measuring stress development during hydrogenation of a metal hydride composite using expanded natural graphite as secondary phase.

Among vertical cylindrical containers, Okumura et al. report an increase of tension as a function of activation cycles, attributed to accommodation of small size particles at the bottom due to the gravity action [18,19]. In another work, porosity was studied in a glass cylinder as a function of activation [20]. A free expansion condition is stated for this study, which might be the case considering the use of glass walls and the low height to diameter ratio of the experimental set-up. From direct observation the authors evaluated the volume increase of hydride bulk as a function of cycle number, showing a gradual increase of porosity as particle size decreases. Furthermore, Dinachandran et al. [21]. studied numerically the occurrence of stresses in the wall of a hydride based hydrogen container. Their simulation does not account for any powder flow but takes into account the porosity distribution of the powder bed.

In these studies, the effect of hydride particle expansion on prototype containers is reported, without studying friction between particles, or between particles and container walls. A recent study of Charlas et al. [22] aimed to improve the understanding of the mechanical behavior of hydrides absorbing and desorbing hydrogen uses a Discrete Element Modelling technique to numerically match experimental measurements of a TiVCr BCC alloy. Rotating drum measurements are introduced, obtaining repose angles about twice the angles presented in this publication, possibly because of the use of different gaseous medium.

Flow behavior of powder materials is a relevant technological issue, usually studied by means of qualitative or quantitative techniques. Moreover, it was suggested that no single technique is suitable for characterization of powder flowability [23]. A complete review of the most common measurement methods is presented by Schwedes and Schulze [24]. It is important to note that studying the hydride powder flowability would require a controlled atmosphere, as it is highly reactive with air, and also to keep a hydrogen pressure to the desired pressure-temperature condition in order to favor an absorbed or desorbed state. Even when there are a number of different quantitative measuring techniques, these usually require the manipulation of powders and the use of sample holders that cannot be easily sealed or pressurized. It is therefore of great importance to know whether flowability can be addressed on hydride forming alloys in desorbed state alone, or if measurements need to be done under hydrogen pressure. In contrast with this, in the rotating drum technique the powder is completely confined within the drum and the apparatus can be modified to withstand hydrogen pressure [25]. The rotating drum technique is used to study powder friction, addressing flowability for industrial processes, such as silo storage, hopper discharge, etc. [26–28]. Shear strength is caused by gravity forces as the powder gets tilted in the rotating drum until a re-accommodation occurs, defining a dynamic angle of repose which is a function of particle friction. Depending on the powder properties, drum size, filling volume fraction and rotating speed, different motion regimes were defined [29]. Although stresses within hydride container could be much greater than in a rotating drum, where powder is unconfined and under constant mixing, this method is suited to measure the angle of repose in a controlled atmosphere making it an excellent candidate for preliminary flowability assessment.

In this work we present a modified rotating drum device to measure flowability of a hydrogen absorbing material under a controlled atmosphere and under different hydrogen concentration states. Using this device we obtained measurements on $LaNi_5$, a well-known hydrogen storage alloy, under different stages of activation in both, absorbed and desorbed state. As a complementary measurement we include the particle size evolution at different activation stages.

Material and methods

Material preparation

To obtain the hydrogen storage material $LaNi_5$, pure elements were melted in an arc furnace under argon (>99.98% purity), using a water-cooled copper crucible, then turned and re-melted five times to improve homogeneity. Once cooled, the alloy ingots were crushed and sieved through a 1400 μm mesh. The resulting powder was sieved through a 74 μm mesh keeping the retained powder. This procedure is aimed at enhancing porosity mitigating alloy contamination while in contact with air. Single $LaNi_5$ phase composition (COD#96-100-0026) was confirmed by XRD technique in a Panalytical Empyrean diffractometer with PIXcel^{3D} detector. Powder diffractograms were obtained at room temperature, using CuKα1 radiation ($\lambda = 1.5406$ Å), in the 10–90° range (2θ) with a 0.013° step.

A basic set of pressure-composition-temperature (PCT) curves was obtained with a Sieverts type device to confirm absorption pressure of the alloy (Fig. 1). From these measurements we defined an absorption pressure of 8 bar for hydride temperatures below 40 °C. Alloy capacity is above

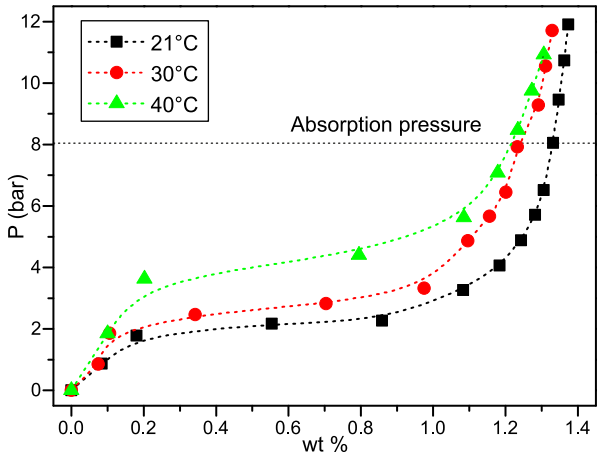

Fig. 1 – Basic alloy characterization.

1.2 wt% (hydrogen mass × 100/hydride mass), as expected for this sort of material.

Every activation cycle consisted of an absorption process (i.e. hydrogen concentration reaching a maximum) followed by a desorption process (i.e. hydrogen concentration reaching a minimum). We call "charged" state at the condition at the end of the absorption process for every activation cycle. Likewise we call "discharged" state at the condition at the end of the desorption process.

Experimental set-up

A rotating drum capable of withstanding 12 bar pressure was designed for the present study. The rotating drum cavity has a diameter of (50.0 ± 0.5) mm and a depth of (15.0 ± 0.5) mm. The cylindrical wall was sandblasted to maximize friction while 10 mm thick float glass was used on both sides to have optical access and to minimize friction. The angular velocity was set to (4.2 ± 0.1) rpm. To inject or extract hydrogen a 0.5 μm nominal passage stainless steel filter was fitted flush with the cylindrical wall. Also an on-off valve and a quick connector were fitted to allow disconnecting the hydrogen supply (Fig. 2). A matt green surface was placed behind the rear glass to enhance imaging contrast.

We performed a hydraulic test up to 12 bar to confirm the front glass resistance. Then we filled the drum with sieved $LaNi_5$ powder, up to approximately 30% of its internal volume (volume of uncompacted material ≈ 8 cm^3). To calibrate the images for the angle of repose calculation we used a home-made plumb and an inclinometer Bosch DNM 60L (resolution ± 0.1°).

The drum was then connected to a Sieverts type device to provide high purity hydrogen (99.999% Linde-AGA Argentina) and to alternatively produce vacuum with a mechanical rotary pump. Room temperature was measured with a Testo 735 prove, and pressure evolution was measured with a PX01A Omega pressure transducer.

Fig. 3 shows a scheme of the experimental set-up.

All handling of the absorbing material from first hydrogen exposure was made under controlled atmosphere in a

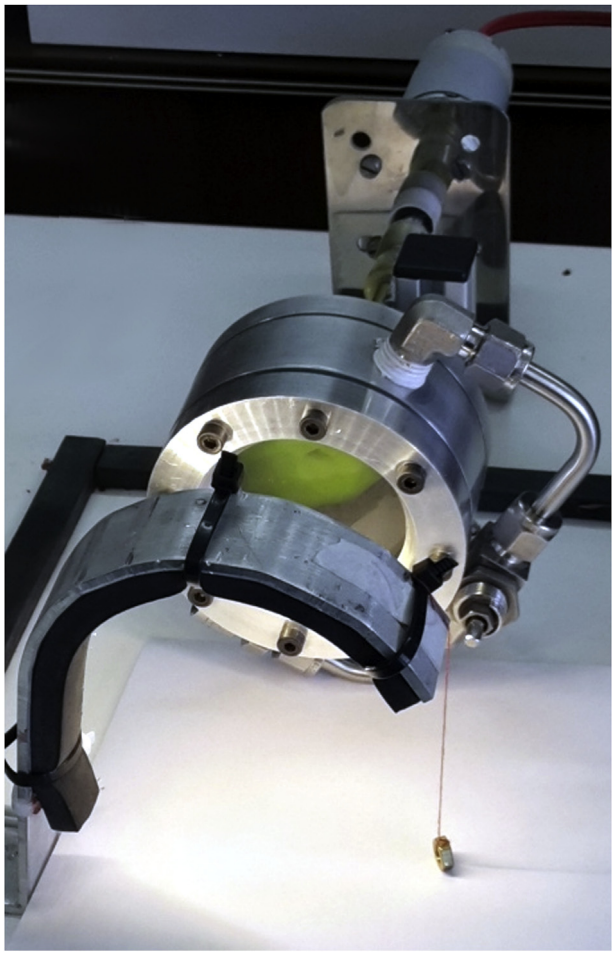

Fig. 2 – Picture of the modified rotating drum.

M-Braun MB10 glove box (oxygen and humidity concentrations ≤ 4 ppm/vol).

Image capture and processing

To evaluate the evolution of dynamic angle of repose as a function of hydride activation, videos were produced with a Nikon 1 J5 camera with a 30–100 mm zoom, obtaining 60 frames per second (f.p.s.). To ensure contrast homogeneity between successive videos we placed a LED light source between the camera and the drum. Image analysis was performed by means of an ad hoc software routine. First, solid–gas interphase profile was detected by color balance analysis, taking to absolute black all points above a certain value of green composition. In case of rolling regime, one linear regression was defined at the edge of the solid–gas interphase, while when the motion regime of the powder showed transition from rolling to slumping, two linear regressions we defined. In order to avoid noise from agglomerates sliding or dropping during avalanche at slumping regime, we defined a minimum goodness of fit condition of $R^2 \geq 0.9$. In the same trend, two domains representative of the phenomena were defined to perform linear

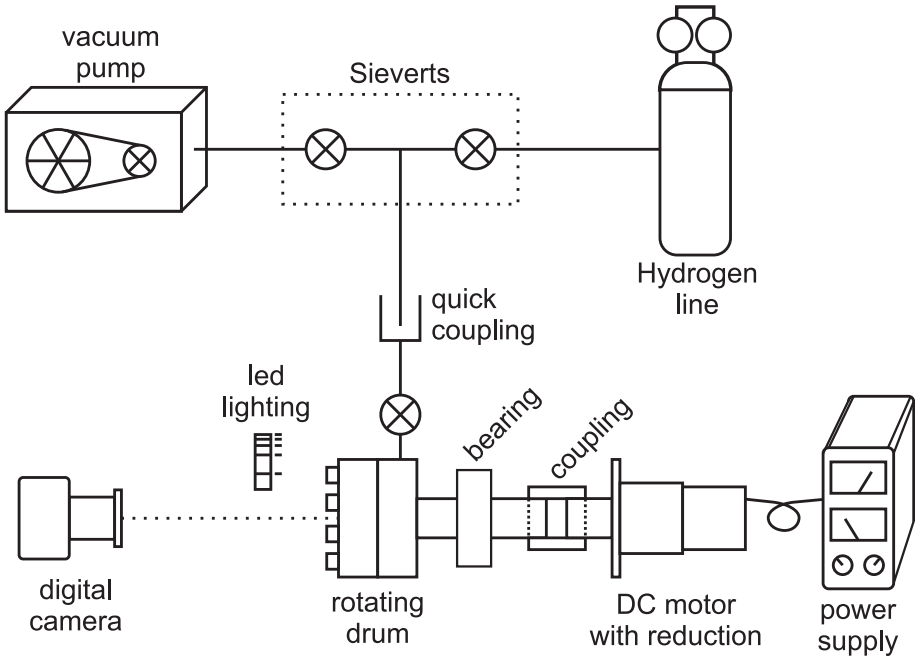

Fig. 3 – Scheme of experimental set-up.

regressions: 9.5%–41% for the lower part of the moving powder interphase and 68%–90.5% for the upper part (α and β in Fig. 4a according to [26]). These two domains are used to obtain the lower angle of repose and upper angle of repose respectively. The systematic error of the angle measurements was addressed based on the roundness of the image of the drum window and on the vertical reference provided by the plumb. This error is estimated to be within ±0.6°. As the frame rate adopted is 60 f.p.s., and the rotating velocity is 4.2 r.p.m., there is a quantification of the angular position of 0.4°. The angle quantification noise is $0.4°/\sqrt{12} = 0.11°$ and can be neglected.

The powder upper and lower angle of repose were plotted based on the processing of more than 6500 images for each activation condition.

Particle size distribution

The reactivity of the hydride powder with water and oxygen from air precludes the use of automated particle size analyzers. We decided to sample the powder in the glove box and load it on a glass sample carrier. The sample carrier was covered with a thin cover glass and the perimeter sealed with an epoxy resin with low gas permeability (Loctite® 1C™ Hysol®). The particle sizes were measured directly from the digital image obtained from a trinocular microscope. The images obtained are 2592 × 1944 pixels, and each pixel is equivalent to 0.252 μm distance. The size was taken as the smallest overall dimension, i.e. the dimension that would allow the particle to pass through the equivalent sieve size. We measured at least 300 particles per sample. In one case the

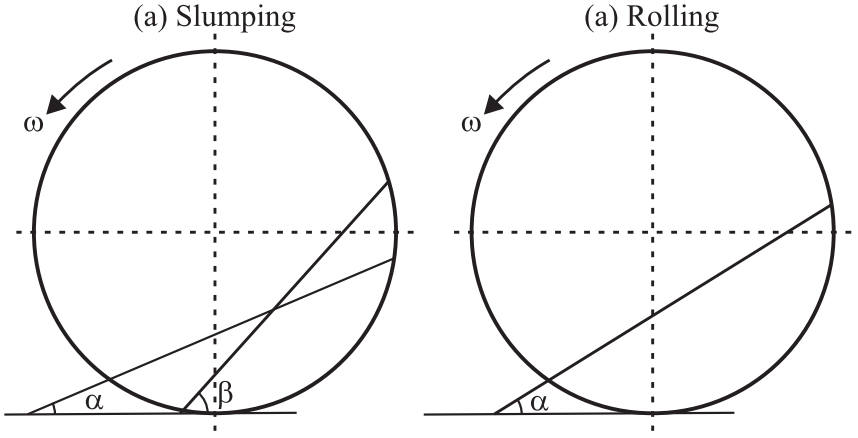

Fig. 4 – Scheme of slumping and rolling motion regimes.

procedure was repeated three times in order to obtain an estimation of repeatability. This value is used as a relative error estimation for all measurements.

Reaction time estimation

In a previous work we defined a method to estimate reaction time for absorption process in hydride containers of some absorbing alloys, including $LaNi_5$ [30]. The method consists of a first calculation to define whether the global process is controlled by kinetics of heat transfer. For the latter case there is a second calculation where reaction time can be readily estimated according to non-dimensional parameters that consider the heat produced during absorption reaction and the heat that the system can dissipate. The expected accuracy of the method is about 20% [31], which is enough to determine reaction time of our experimental set-up.

Based on these calculations we adopted a reaction time no less than 180 min for the absorption process and 45 min for the desorption process. Further details of the pressure conditions of activation, and assumptions made to estimate desorption reaction time can be found in Annex A.

Results and discussion

The images obtained by optical microscopy for cycles 2, 5 and 20 are shown in Fig. 5. The shape of the observed particles are either triangular or square with sharp edges, as expected in a fragile size reduction for this type of alloy. We verified that the particles are not flat, i.e. flakes, by doing a multi-focus image processing of the particles. The height of the particles laying on the sample carrier is similar to the smallest dimension of the particles as seen through the microscope.

Using the measured sizes we calculated the threshold sizes corresponding to the 10%, 50% and 90% cumulative volume, Dv10, Dv50 and Dv90 respectively. The values obtained for the samples taken at different cycle numbers are shown in Fig. 6. It can be observed that the larger particles continue being reduced after cycle number 10, as reflected in the decreasing Dv90, while Dv50 values show only a minor reduction.

As the powder particle size is reduced, small particles begin to stick to other particles. The samples were sonicated and vibrated to achieve the best possible dispersion, but it is likely that the Dv10 size is somewhat overestimated due to the agglomeration of the smallest particles.

Fig. 7 depicts the interphase angles for every imaging frame obtained during each measurement for discharged state of all activation cycles normalized to the frequency of appearance.

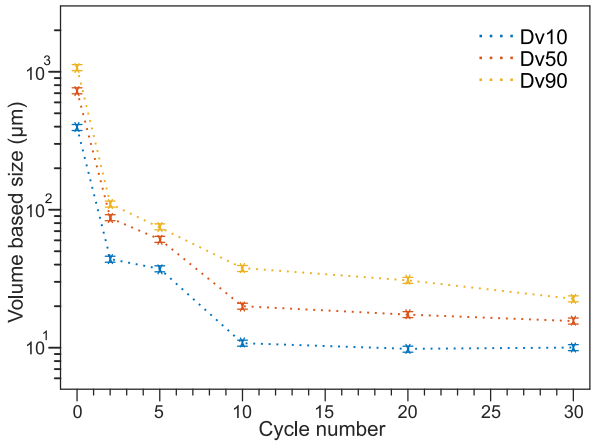

Fig. 6 – Cumulative volume evolution as a function of cycle number.

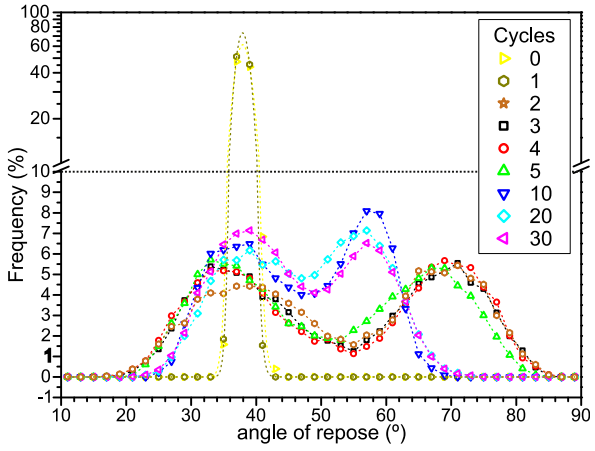

Fig. 7 – Angle of repose of discharged measurements.

We added a Gaussian fitting function as a visual aid. The general behavior of powder as activation evolves can be divided in three stages: i) cycles 0 and 1 showing very shallow angles, indicating good flowability. Rolling regime is observed at this initial stage. A single dynamic angle of repose appears for every cycle in the image analysis, as shown in Fig. 8a. ii) Cycles 2–5 with slumping regime. The presence of α and β angles of repose is clear from the two-hill shape of this group of curves. iii) Cycles 10, 20 and 30 show the same behavior as cycles 2–5, with a slumping regime, but here there is a marked displacement of β angles of repose to lesser values, suggesting

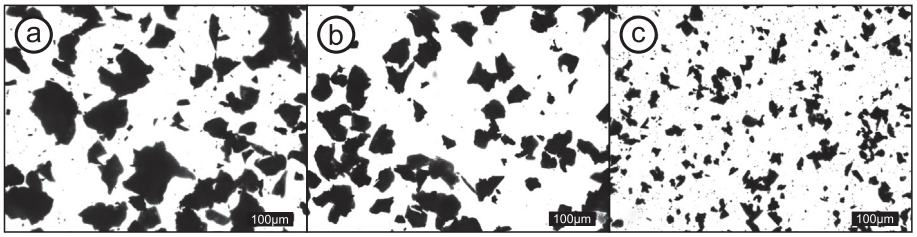

Fig. 5 – Trinocular microscope images for a) cycle 2, b) cycle 5 and c) cycle 20.

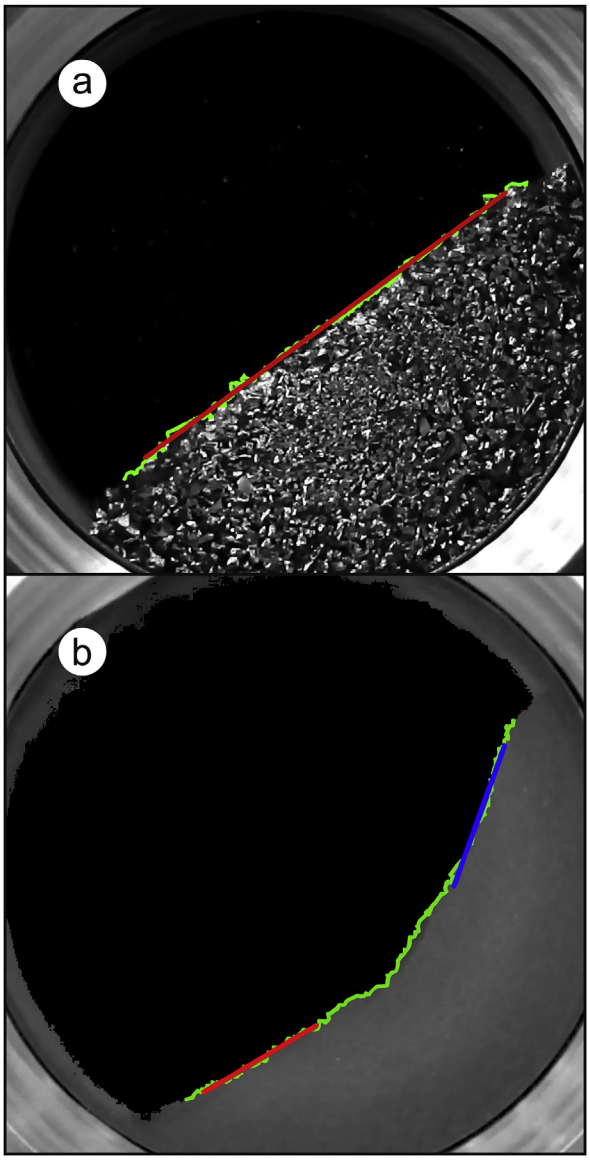

Fig. 8 – Single frame image after processing for a) cycle 0 and b) cycle 30.

less cohesivity between particles, as will be discussed later. Fig. 8b shows one frame of the cycle 30 after image processing, where solid gas interphase is brought out in green, and α and β angles of repose are shown in red and blue respectively. Particle size reduction is also evident in Fig. 8. From a qualitative point of view, Figs. 7 and 8 point out that powder cohesivity evolves with activation, and that there is a stabilization tendency for the higher cycles analyzed.

We observed an important volume expansion (28%) between cycle 1 and 2 due to porosity increase. A detailed study of hydride expansion during activation is presented by Matsuchita et al. [32]. Before proceeding, we removed part of the hydride powder in the glove box, maintaining ≈ 8 cm^3 for the entire set of experiments. Flow regime change from cycle 2 is consistent with this abrupt change in powder characteristics.

Rolling and slumping regimes are in accordance with regime prediction defined in Ref. [29], considering that centrifugal forces are negligible respect to gravitational forces (in our experimental set-up, Froude number is 2.5×10^{-5}). Slumping regime outcomes bring abundant data points, particularly when analyzing separately α and β angles of repose. Still, Fig. 7 does not reveal that each avalanche produced in this regime has a single maximum β angle right before the avalanche, and a single minimum α angle after powder displacement stops. Given that maximum β angle and minimum α angle are better suited to address powder flowability, we isolated them to further analyze our results in a more quantitative way. We obtained the angles shown in Fig. 9 for the lower angle of repose, and Fig. 10 for the upper angle of repose, both in discharged and charged conditions. Cycles 10, 20 and 30 where measured in discharge state, while cycles 11, 21 and 31 were measured in charged state. Each curve shown in these figures include a minimum of 150 measurements, obtained by analyzing angle of repose

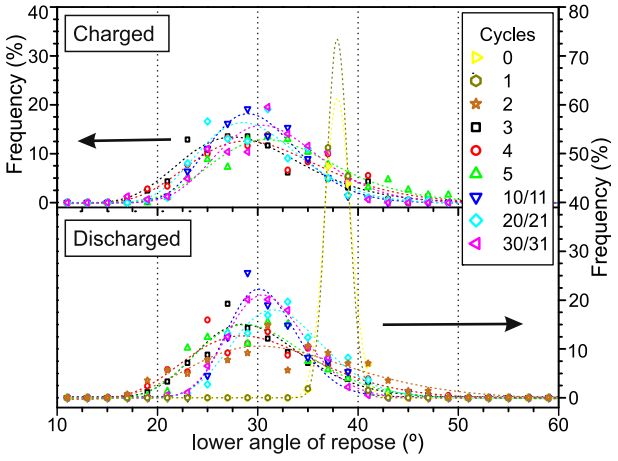

Fig. 9 – Lower angle of repose for discharged and charged condition (upper curves correspond to left vertical axe, while lower curves correspond to right vertical axe).

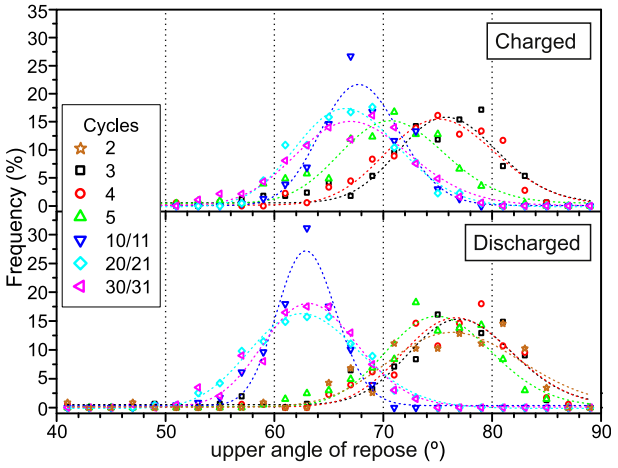

Fig. 10 – Upper angle of repose for discharged and charged condition.

change for successive frames from image processing outcomes.

Results depicted in Fig. 9 for the lower angle of repose show little variation of the angle of repose with cycle number in the slumping regime cases, without revealing an obvious tendency for the charged condition. For the discharged condition there is a slight tendency to higher angle values with cycle number. Fig. 10 instead shows a more noticeable difference when compared to the previous figure. Both for the discharged and charged states there is a tendency of decreasing upper angle of repose as activation evolves. Particularly cycle 5 confirms this tendency by separating from cycles 2, 3 and 4, and approaching the angles obtained for the cycles 10, 20 and 30. The standard deviation of the measurement of the angle of repose for slumping regime is approximately 10°, and we have taken no less than 150 events for each case. The statistical error can therefore be estimated as $\sim 10^\circ/\sqrt{150} \approx 1^\circ$.

We think that this behavior can be due to the generation of sub-micron particles that would act as flow agents for the bigger particles. If present, these smaller particles stick to bigger ones increasing distance, thus reducing van der Waals adhesive forces, leading to a less cohesive powder behavior. According to Schulze [33], added flow agent particles generally have a particle size range from 5 nm to 100 nm, and a concentration below 1 wt%. Sub-micron particles have been observed in hydride systems in previous works [34–36], reinforcing our hypothesis. The absence of sub-micron size particles in Fig. 5 is related to optical microscopy resolution limitations. The verification of this hypothesis, for example by SEM analysis, would require a special system to avoid exposing the metal hydride to air, and will be pursued in a future work.

In the upper angle of repose case a different behavior in charged and discharged states can be observed. It is of particular interest a difference of ≈4° at cycles 10, 20 and 30, as shown in Fig. 10. This outcome indicates a measurable difference that cannot be attributed to the error of the technique. Nonetheless it should be noted that powder flowability depends on the density of the powder, as reflected for example in the use of the Geldart criteria [37] for powder flowability assessment. In our device the shear tensions are originated by the force of gravity acting on the powder. There is a significant density change between charged and discharged states that are expected to influence our results. Further studies need to be done to address which material properties determine the flowability change between the charged and discharged states.

Conclusions

$LaNi_5$ particles flowability was studied during the activation process by the rotating drum technique. The modified drum device allowed us to charge and discharge the hydrogen absorbing material and perform direct measurements of dynamic angle of repose, which is an indicator of powder flowability.

The absorbing material sample was sieved before being loaded into the device, and showed no major changes after cycle 1. Then from cycle 2 onwards the flow regime changed as particle size reduced, from an initial rolling regime to a slumping regime, with well-defined upper and lower angles of repose. The smaller particle size obtained at cycles 2– 5 justify a more cohesive behavior when compared to initial sample. Still, cycles 10, 20 and 30 show a tendency to a smaller angle of repose when compared to cycles 2–5. This angle of repose reduction can be seen as an improvement in powder flowability.

In comparison to activation, hydrogen concentration has a lesser influence in angle of repose. From upper angle of repose measurements it is observed a difference of approximately 4° between discharged and charged states, which may be related to density change. Thus, we can conclude that the flowability of the hydride forming alloy does not change dramatically between the discharged and charged states.

As future activities we envisage addressing the sub-micron particle content of particles acting as flow agents, and the introduction of added flow agents for hydrogen absorbing powders.

Acknowledgements

Authors want to thank the following Argentinean institutions for financial support: CNEA, Conicet and ANCyT (project codes PICT-1510-2012 and PICT 1403-2013).

Annex A

In the present work we performed absorption–desorption cycles inside the rotating drum, with a maximum operational pressure of ≈8 bar (cycles 0–5), and inside the reaction chamber of the Sieverts device, with a maximum pressure of ≈40 bar (cycles 6–31). In both cases minimum pressure was the vacuum produced by a mechanical pump at the end of the desorption process ($P \leq 4 \times 10^{-2}$ mbar). Table AI indicates common values of the parameters used for calculations according to the method presented in Ref. [31], and Table AII shows results for absorption and desorption processes under the named pressure conditions.

The bottom line of Table AII indicates sorption reaction time for every process and for every reactor according to estimated reaction time.

The non-dimensional method taken from our previous study [31] is defined for absorption process, but we also use it to estimate the desorption time by doing the following assumptions: i) $LaNi_5$ kinetics and enthalpy change for absorption and desorption processes are comparable, ii) the parameter T_{ext} has its correspondent P_{eq} value according to Van't Hoff equation. The same equivalence occurs between system pressure P_g and the maximum temperature T_{max} that an isolated system could reach with the hydride absorbing at that pressure. Thus, pressure and temperature of the reacting system are both driving forces that can be taken to its equivalent (i.e. T_{ext} to P_{eq} and P_g to T_{max}). Then, by knowing the desorption temperature of the hydride container, we estimated the equivalent equilibrium pressure (P_{eq}^{deso}) expected for an absorption process.

Since the actual driving force for pressure is vacuum pressure ($P_{vacuum} = 0$ bar), the equivalent ΔP of a desorption process is considered to be:

$$\Delta P = P_{eq}^{deso} - P_{vacuum} \quad (A1)$$

Nonetheless, in order to use the non-dimensional method without producing pressure values equal to zero, which invalidates the equations, we estimated an equivalent system pressure P_g^{deso}. This value is estimated as the double of P_{eq}^{deso}, so that the ΔP value of equation (A1) remains the same:

$$\Delta P = P_g^{deso} - P_{eq}^{deso} \quad (A2)$$

Finally, with this equivalent system pressure we estimated an equivalent maximum temperature T_{max}^{deso} of the system. With these new parameters, desorption reaction time can be estimated following the same procedure as for absorption process, replacing equations (7) and (8) of [31] by the following equivalent equations:

$$NDC^{deso} = \frac{\dot{Q}_{dis}^{deso}}{\dot{Q}_{rea}} \quad (A3)$$

$$\dot{Q}_{dis}^{deso} = \frac{\left(T_{max}^{deso} - T_{ext}\right)}{L/k_{eff}} \quad (A4)$$

Table AI – Parameters used in reaction time calculations.

Parameter	Value
k_{eff} ($W \cdot m^{-1} \cdot K^{-1}$)	1
ΔH ($J \cdot mol^{-1}$)	27024
C_{MH} ()	0.013
ρ_0 ($kg \cdot m^{-3}$)	8300
1-ε ()	0.55
1-F ()	1
MW_{H2} ($kg \cdot mol^{-1}$)	0.002015
f_{FC} ()	0.43
κ_{abs} (s^{-1})	59.2
E_{abs} ($J \cdot mol^{-1}$)	21170

REFERENCES

[1] Züttel A. Materials for hydrogen storage. Mater Today 2003:24–33.

[2] Using metal hydride to store hydrogen". Heung L. sitio web: http://sti.srs.gov/fulltext/.

[3] Jepsen J, Bellosta von Colbe JM, Klassen T, Dornheim M. Economic potential of complex hydrides compared to conventional hydrogen storage systems. Int J Hydrogen Energy 2012;37:4204–14.

[4] Au Ming, Wu Jing, Wang Qi-Dong. Some engineering methods for eliminating deformation and expansion damage of hydride storage containers. J Less-Common Metals 1991;172–174:1168–74.

[5] Khandelwal A, Agrsti F, Capurso G, Lo Russo S, Maddalena A, Gialanella S, et al. Pellets of MgH2-based composites as practical material for solid state hydrogen storage. Int J Hydrogen Energy 2010;35:3565–71.

[6] Sandia laboratories files, web site: http://hydpark.ca.sandia.gov/Reference_introgrn.html#top.

[7] Qin Feng, Chen Jiangping, Chen Zhijiu. The hydriding–dehydriding characteristics of La0.6Y0.4Ni4.8Mn0.2 and their influences in the surface strain on small-scale, thin-wall and vertical containers. Mater Des 2008;29:1926–33.

[8] Lin Chih-Kuang, Huang Sih-Ming, Jhang Yu-Hao. Effects of cyclic hydriding–dehydriding reactions of Mg2Ni alloy on the expansion deformation of a metal hydride storage vessel. J Alloys Compd 2011;509:7162–7.

[9] Herbrig K, Röntzsch L, Pohlmann C, Weißgärber T, Kieback B. Hydrogen storage systems based on hydride graphite composites: computer simulation and experimental validation. Int J Hydrogen Energy 2013;38:7026–36.

[10] Duan W, Du J, Wang Z, Niu Y, Huang T, Li Z, et al. Strain variation on the reaction tank of high hydrogen content during hydrogen absorption desorption cycles. Int J Hydrogen Energy 2013;38:2347–51.

[11] Lototskyy MV, Davids MW, Tolj I, Klochko YV, Sekhar BS, Chidziva S, et al. Metal hydride systems for hydrogen storage and supply for stationary and automotive low temperature PEM fuel cell power modules. Int J Hydrogen Energy 2015;40:11491–7.

[12] Ribeiro E, Gil J. A novel capacitive device for the study of volumetric expansion of hydride powders. Int J Hydrogen Energy 2015;40:14900–10.

[13] McKillip T, Banister C, Clark E. Stress analysis of hydride vessels used for tritium storage. Fusion Technol 1992;21:1011.

Table AII – Reaction time estimations for different conditions.

	Rotating drum		Sieverts reactor	
	Absorption	Desorption	Absorption	Desorption
L (m)	0.01	0.01	0.01	0.01
NDK	30.7	28.4	29.2	31.7
Governing process	Heat transfer	Heat transfer	Heat transfer	Heat transfer
P_g (bar)	9.0	$P_g^{deso} = 15.3$	40	$P_g^{deso} = 18.5$
T_{ext} (°C)	20	20	25	25
T_{max} (°C)	24.1	$T_{max}^{deso} = 39.4$	71.1	$T_{max}^{deso} = 45.1$
P_{eq} (bar)	7.7	$P_{eq}^{deso} = 7.7$	9.2	$P_{eq}^{deso} = 9.2$
NDC	0.016	0.073	0.17	0.07
NDFT	27.8	5.89	2.48	5.68
$t_{90\%}$ (min)	138.4	29.4	12.4	28.4
$t_{process}$ (min)	**≥180**	**≥45**	**≥30**	**≥60**

[14] Nasako K, Ito Y, Hiro N, Osumi M. Relaxation of the internal stress generated in the hydrogen absorbing alloy vessels. Int J Hydrogen Energy 1998;23(10):921–9.
[15] Nakano A, Maeda T, Ito H, Motyka T, Perez-Berrios JM, Greenway S. Experimental study on a metal hydride tank for the totalized hydrogen energy utilization system. Energy Procedia 2012;29:463–8.
[16] Hass I, Schütt E. The effect of mechanical stress on the absorption of hydrogen by metal hydrides. Int J Hydrogen Energy 1991;16(12):815–20.
[17] Heubner F, Pohlmann C, Mauermann S, Kieback B, Röntzsch L. Mechanical stresses originating from metal hydride composites during cyclic hydrogenation. Int J Hydrogen Energy 2015;40:10123–30.
[18] Okumura Masahiko, Terui Koki, Ikado Ayaka, Saito Yasuhiro, Shoji Masakazu, Matsushita Yohsuke, et al. Investigation of wall stress development and packing ratio distribution in the metal hydride reactor. Int J Hydrogen Energy 2012;37:6686–93.
[19] Okumura Masahiko, Ikado Ayaka, Saito Yasuhiro, Aoki Hideyuki, Miura Takatoshi. Pulverization mechanism of hydrogen storage alloys on microscale packing structure. Yoshiaki Kawakam Int J Hydrogen Energy 2012;37:10715–23.
[20] Matsushita Masahiro, Monde Masanori, Mitsutake Yuichi. Experimental formula for estimating porosity in a metal hydride packed bed. Int J Hydrogen Energy 2013;38:7056–64.
[21] Dinachandran L, Mohan G. Numerical simulation of the parametric influence on the wall strain distribution of vertically placed metal hydride based hydrogen storage container. Int J Hydrogen Energy 2015;40:5689–700.
[22] Charlas B, Kneib F, Gillia O, Imbault D, Doremus P. A tool for modelling the breathing of hydride powder in its container while cyclically absorbing and desorbing hydrogen. Int J Hydrogen Energy 2015;40:2283–94.
[23] Krantz Matthew, Zhang Hui, Zhu Jesse. Characterization of powder flow: static and dynamic testing. Powder Technol 2009;194:239–45.
[24] Schwedes J, Schulze D. Measurement of flow properties of bulk solids. Powder Technol 1990;61(1):59–68.
[25] Rietema K, Cottaar W. The effect of interstitial and circumambient gas in fine powders on the scaling up of powder-handling apparatus as illustrated by ball mill operation. Powder Technol 1987;50:147–54.
[26] Liu Xiao Yan, Specht E, Mellmann J. Experimental study of the lower and upper angles of repose of granular materials in rotating drums. Powder Technol 2005;154:125–31.
[27] Geldart D, Abdullah EC, Verlinden A. Characterisation of dry powders. Powder Technol 2009;190:70–4.
[28] Pirard S, Lumay G, Vandewalle N, Pirard J-P. Motion of carbon nanotubes in a rotating drum: the dynamic angle of repose and a bed behavior diagram. Chem Eng J 2009;146:143–7.
[29] Mellmann J. The transverse motion of solids in rotating cylinders-forms of motion and transition behavior. Powder Technol 2001;118:251–70.
[30] Melnichuk M, Silin N. Guidelines for thermal management design of hydride containers. Int J Hydrogen Energy 2012;37:18080–94.
[31] Silin N, Melnichuk M. A case study of a hydride container performance applying non dimensional parameters. Int J Hydrogen Energy 2014;39:21060–7.
[32] Matsushita M, monde M, Mitsutake Y. Experimental formula for estimating porosity in a metal hydride packed bed. Int J Hydrogen Energy 2013;38:7056–64.
[33] Schulze D. Powders and bulk solids – behavior, characterization, storage and flow. ISBN 978-3-540-73767-4. Ed. Springer; 2008. p. 211–5.
[34] Hirohisa Uchida, Uchida Haruhisa, Huang Yen C. Effect of the pulverization of LaNi5 on the hydrogen absorption rate and the X-ray diffraction patterns. J Less Common Metals 1984;101:459–68.
[35] Joubert JM, Latroche M, Černý R, Percheron-Guégan A, Yvon K. Hydrogen cycling induced degradation in $LaNi_5$-type materials. J Alloys Compd 2002;330:208–14.
[36] Hahne E, Kalleweit J. Thermal conductivity of metal hydride materials for storage of hydrogen: experimental investigations. Int J Hydrogen Energy 1998;23(2):107–14.
[37] Geldart D. The effect of particle size and size distribution on the behaviour of gas-fluidised beds. Powder Technol 1972;6(4):201–15.